Large-Scale Experiments on the Formation of Surface Vortices with and without Vortex Suppression

Nicolai Szeliga*, Lando Helmrich von Elgott, Daniel Bezecny, Steffen Richter, Marko Hoffmann, and Michael Schlüter

DOI: 10.1002/cite.201900091

Experiments were carried out in a 50-m^3 cylindrical tank to determine the influence of strong momentum on the formation of large-scale gas-core vortices. Gas-core lengths were measured for varying volume flow rates and submergence depths. The critical Froude numbers were also determined and the efficiency of different vortex suppressors on the gas-core formation was investigated. The horizontal velocity field inside the vortex core region was additionally recorded using particle image velocimetry. The experimental results were used to verify numerical simulations and compared to vortex models and correlations from literature.

Keywords: Circulation, Free surface vortex, Gas entrainment, Pumps, Vortex suppression

Received: June 19, 2019; *accepted:* October 10, 2019

1 Introduction

The occurrence of surface vortices in pump intakes represents a safety hazard for the reliable operation of cooling circuits in industrial facilities, such as chemical reactors, power plants, and hydroelectric power stations. Surface vortices are a major cause for gas entrainment into the pump system, where the gas can accumulate inside the pump head and lead to a reduced pump capacity. Ultimately, gas accumulation can even lead to the complete breakdown of the cooling circuit if enough gas accumulates inside the impeller blades of the pump. In case of emergency cooling and residual heat removal systems in nuclear power plants as well as for cooling systems used in exothermic reactions, this can cause great harm to the plant as well as the environment due to a thermal runaway of the reactor. Even before a critical gas amount can cause a breakdown, gas bubbles might cause cavitation damages in system components, such as impellers or valves.

Rotating gas-core vortices occur on the surface of a liquid volume when liquid is withdrawn with a high velocity relative to the liquid level. The withdrawal causes a pressure drop in the liquid above the pump intake and liquid will flow towards the pump intake. When the liquid level above the pump intake is large in comparison to the pump intake diameter, inhomogenities in the inflowing liquid will cause the liquid bulk phase to circulate around the pump intake, forming a vortex [1]. The pressure drop at the surface thereby determines the depth of the gas core. The strength of the vortex as well as the length of the forming gas core depend on various parameters, most notably the pump intake diameter, submergence, and orientation, the volume flow rate, and the circulation strength. Additional factors can be the shape of the liquid reservoir, the amount of pump intakes within close proximity and induced tangential momentum, through inlet pipes, rakes, or obstructions in the inflow.

Vortices can be divided into different categories according to the length of the forming gas core, using a six-level classification proposed by Hecker: 1) subsurface rotation, 2) forming of first surface dimple, 3) vortex core reaches into the pump intake, 4) entrainment of particles at the gas-core tip, 5) start of gas (bubble) entrainment into the pump intake, 6) critical vortex condition – gas core reaches into the pump intake [2]. The development and strength of gas-core vortices in pump intakes is challenging to predict, due to the huge variety of possible intake geometries, sizes and inflow conditions as well as the complex fluid dynamic phenomena occurring during vortex formation. Intensive investigations on the vortex formation in varying scales have been conducted by Anwar [3, 4], Daggett & Keulegan [5], Jain et al. [6], Rindels and Gulliver [7], and Hecker [2]. Large-scale particle image velocimetry measurements have

Nicolai Szeliga, Lando Helmrich von Elgott, Daniel Bezecny, Steffen Richter, Dr.-Ing. Marko Hoffmann, Prof. Dr.-Ing. Michael Schlüter
nicolai.szeliga@tuhh.de
Technische Universität Hamburg, Institut für Mehrphasenströmungen, Eißendorfer Straße 38, 21073 Hamburg, Germany.

already been made by Keller et al., but in a setup with horizontal intake orientation [8].

2 Theoretical Background

2.1 Theoretical Vortex Models

The fluid dynamics behind gas-core vortices and their formation have been a topic of research for a long time, starting with the first model by Rankine in 1858 [9]. In his model, Rankine describes the vortex flow as a rigid body rotation in the center and a potential vortex in the outer regions. Roughly a century later, a single-phase vortex model was developed by Burgers [10] and later refined by Rott [11], based on a simplification of the Navier-Stokes equation. With the model, the azimuthal velocities inside a free surface vortex

$$u_\theta(r) = \frac{\Gamma_\infty}{2\pi r}\left[1 - \exp\left(-\frac{ar^2}{2\nu}\right)\right] \tag{1}$$

can be calculated for a symmetrical and time independent system. For the calculation of the azimuthal velocity profile only two parameters are needed: the first parameter is the bulk circulation Γ_∞, which is the circulation outside the vortex core region, where the potential flow is dominant and, therefore, the circulation around a closed curve c

$$\Gamma = \oint_c u\mathrm{d}r \approx 2\pi u_\theta r \tag{2}$$

is constant. The second parameter needed for the azimuthal velocity is the axial acceleration within the vortex core region, defined as

$$a = \frac{4\nu}{r_0^2} \tag{3}$$

derived from the kinematic viscosity of the liquid ν, divided by the vortex core radius squared r_0^2 [12]. Note that Rott defines the axial acceleration as $a = 2\nu/r_0^2$ [11], while Odgaard defines the axial acceleration (named proportionality factor) as $a = \nu/2S$ for a critical gas-core vortex [13]. In this paper, the authors decided to use the definition of Ito et al. (Eq. (3)) for all calculations. Bulk circulation and axial acceleration can be used to calculate the length

$$L = (h(r=\infty) - h(r=0)) = \frac{a\ln(2)}{\nu g}\left(\frac{\Gamma_\infty}{4\pi}\right)^2 \tag{4}$$

of a theoretically occurring gas-core vortex [12]. Since the measurement of the undisturbed velocity profile requires the use of (laser)optical measurement techniques, the applicability of the model is normally restricted to laboratory and pilot plant setups or the conduction of numerical simulations. In situ velocity measurement techniques, like hot wire anemometry, are not recommended as they would change the inflow conditions and, therefore, the whole vortex development.

2.2 Correlations for the Critical Submergence

As a more practical approach, correlations for the prediction of the critical submergence have been developed for various intake geometries. The correlations are used to predict the minimal submergence needed to prevent gas entrainment into the pump intake at a given volume flow rate.

A widely used correlation is the correlation given by the Hydraulic Institute's "American National Standard for Rotodynamic Pumps for Pump Intake Design" [14]

$$\frac{S_{\mathrm{crit}}}{D} = 1 + 2.3F \tag{5}$$

which is based on a correlation developed by Hecker [2] and validated for a broad range of intake structures with different sizes and shapes. The critical submergence S_{crit} is defined as the submergence for which a gas-core vortex would reach the opening of the pump intake. In the correlation, S_{crit} is only depending on the intake diameter D and the intake Froude number F

$$F = \frac{u}{\sqrt{gD}} \tag{6}$$

The correlation is a simple but rough tool to determine critical operation conditions if the circulation and the vortex structures are not measureable or for geometries, in which unsteady vortices occur. The applicability of the model is limited to flows with low to moderate circulations, using the intake velocity u and the velocity of the approaching flow as limitations. The limits lie between 1.5 and 2.4 $\mathrm{m\,s^{-1}}$ for the intake and between 0.9 and 1.2 $\mathrm{m\,s^{-1}}$ for the approaching flow velocities, with exact values depending on geometry and size of pump intake and basin [14]. If the intake velocity is above the limit for the specific intake geometry, the installation of vortex suppressors in the pump intake is recommended by the Hydraulic Institute. Larger pump systems with intake volume flow rates of $Q > 1130\,\mathrm{m^3h^{-1}}$ require verification studies with a physical model, according to [14].

2.3 Vortex Suppressors

In an attempt to not only predict the critical submergence depth, but to actively avoid gas-entrainment into pump systems, several authors propose the implementation of static vortex suppressors, see Auckland [15], Trivellato [16], Borgei and Kabiri-Samani [17] as well as the Hydraulic Institute's "American National Standard for Rotodynamic Pumps for Pump Intake Design" [14].

Vortex suppressors are static installations in the shape of bell mouths, crosses, or baffles, which are placed into or above pump intakes. The goal is to minimize the rotational momentum through cross shapes and reduce the pressure drop maximum at the liquid surface, which causes the gas core to form. Based on the work of Padamanabhan [18], the American National Standard recommends horizontal baffles, crosses, or cross-baffle combinations implemented above the pump intake to suppress the vortex formation [14].

To quantify the efficiency of different vortex suppressor types and sizes and to verify the recommendations of the American National Standard for a setup with strong circulations, different vortex suppressors are constructed and characterized at the Institute of Multiphase Flows, as described in the following.

3 Experimental Setup and Conducted Measurements

3.1 Experimental Setup

The experiments are conducted in an industrial-scale setup, erected in the technical center of the Institute of Multiphase Flows at Hamburg University of Technology (TUHH). The experimental plant consists of a cylindrical pump reservoir made from coated carbon steel, while the piping consists of PVC-U pipes with a diameter of DN200 (PN10). The reservoir has a diameter and height of 4 m and can hold a total volume of 50 m^3. For the experiments, the reservoir is filled to varying heights with water. The exact height is measured with a measuring rod. Optical accessibility into the reservoir is given by 24 round borosilicate glass windows, which are equally distributed in three rows around the circumference of the reservoir. Photographs of the setup are shown in Fig. 1.

The plant is operated as a loop flow, with a vertical downward pump intake installed inside the reservoir at a height of h = 1.25 m. From the intake, the water is flowing through a 90° bend and a horizontal pipe to the installed centrifugal pump (KSB-MegaCPK 300-250-315). Behind the pump, the water flows through a heat exchanger and is then split evenly into four separate streams. Each stream is measured by an electromagnetic flowmeter (ABB FEX311) before it flows back into the reservoir. The four entry pipes inside the reservoir are arranged in a circular array around the circumference and bend to face the wall in a vertical angle of β = 45°. Fig. 2 shows a 3D flowchart and a cross-sectional view of the setup. The setup consists of the following parts: 1) pump reservoir, 2) optical access point – suction pipe, 3) pump – KSB MegaCPK, 4) shell and tube heat exchanger, 5) magneto-inductive flow meter – ABB FEX311 (4×). The pipe openings are located below the water surface to avoid bubble generation. For some experiments, an intermediate floor was installed over the whole cross section of the tank at the same height as the pump intake to create a flat bottom without protruding pump intake. The pump intake is an open tube with sharp edges, enabling the installation and investigation of different vortex suppressors. The installed vortex suppressors can be seen in Fig. 3. Six different vortex suppressors have been implemented: funnel, sieve, 45° bend, cross, and two cross baffles of different diameter (2D and 4D).

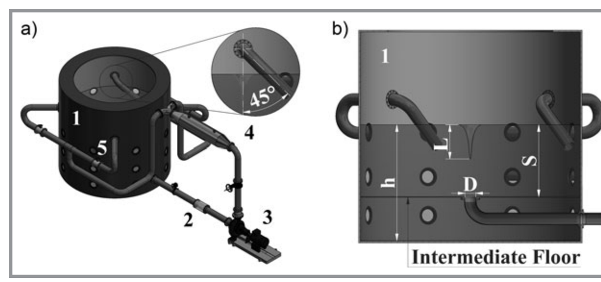

Figure 2. 3D flowchart of the pilot plant in a) isometric and b) cross-sectional view. The setup consists of the following parts: 1) pump reservoir, 2) optical access point – suction pipe, 3) pump – KSB MegaCPK, 4) shell and tube heat exchanger, 5) magneto-inductive flow meter – ABB FEX311 (4×).

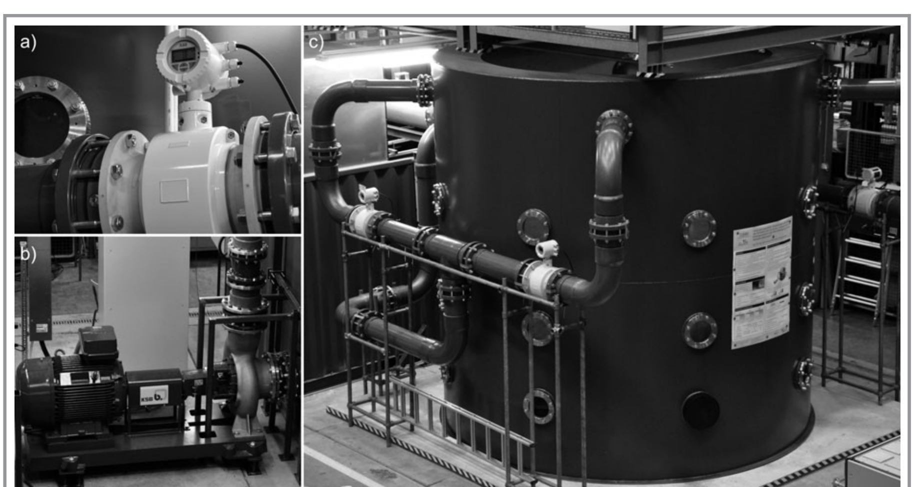

Figure 1. Experimental setup: a) electromagnetic flowmeter ABBFEX311, b) centrifugal pump KSB MegaCPK, and c) cylindrical reservoir.

3.2 Investigation of Gas-Core Lengths

For the investigation of the gas-core length, a camera is attached to one of the access windows and a 1000-W spotlight is orthogonally aligned to it in front of another window. For calibration, a target picture is recorded before each measurement. Likewise, the recordings are only started after a stable gas core has formed and the system has reached steady-state conditions. All recordings are evaluated with Matlab to automate the process and exclude human error in the evaluation

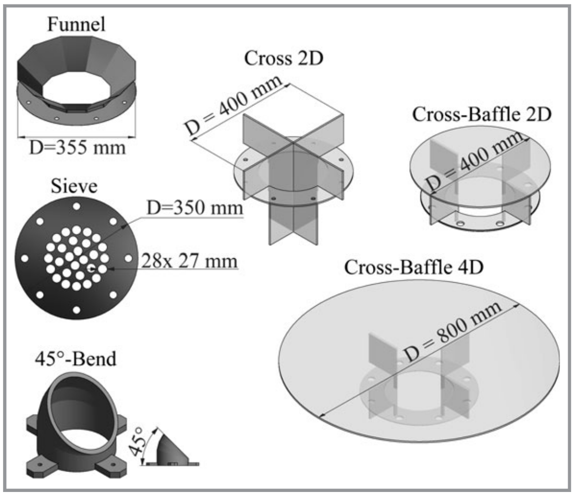

Figure 3. Investigated vortex suppressors.

process. Randomly selected measurements are additionally evaluated by hand, using the free software ImageJ, to confirm the automatically evaluated results. For each measurement, a sample size of 60 images is recorded with a measurement frequency of 1 Hz.

Experiments are conducted for three different submergence depths S = 1.1, 1.5, and 2.1 m. First, without vortex suppressors and Froude numbers ranging from F = 0.4 to 1.8. Then, with vortex suppressors and Froude numbers from F = 0.2 to 4.6. Tab. 1 lists all experimental parameters and fluid properties. Each measurement point is measured twice, to exclude external influences from the results. For the comparability of the dimensionless gas-core lengths at different submergence levels, a dimensionless gas-core length

$$L^* = LS^{-1} \quad (7)$$

is used, dividing the measured gas-core lengths by the corresponding submergence depths. The values of L^* are between 0, where no gas core has formed yet, and 1, where the tip of the gas core reaches the pump intake. At this point, the critical submergence depth $S = S_{crit}$ is reached.

For selected experiments, dye core experiments are conducted by inserting 1 L of blue ink into the vortex center. This enables a qualitative description of the flow structures above the pump intake.

Table 1. Fluid properties and experimental parameters at 20 °C and 1.013 bar.

Parameter	Value
Volume flow rate Q [m^{3}h^{-1}]	32–730
Pump intake velocity u [m s^{-1}]	0.3–6.5
Pump intake Froude number F [–]	0.2–4.6
Kinematic viscosity (water) ν [m^{2}s^{-1}]	$1.004 \cdot 10^{-6}$
Density (water) ρ [kg m^{-3}]	998.2
Submergence depth S [m]	1.1–2.1
Vertical inflow angle β [°]	45
Pump intake diameter D [m]	0.2

3.3 Particle Image Velocimetry

Particle image velocimetry (PIV) measurements are conducted for a submergence depth of S = 1.5 m and a Froude number of F = 0.5. A pulsed high-power LED was used as a light source and polyamide particles (EMS-Griltech Griltex® 1A, D_p = 80–200 μm) as seeding particles [19]. The LED is used instead of a pulsed laser, due to safety concerns, as the setup could not be shielded completely against emitting light to the surroundings. The LED is mounted in front of one of the glass windows, emitting blue light with a wavelength of λ = 454 – 462 nm. The light beam generated by the LED is focused into a narrow slit through two lenses (half-sphere and cylinder) placed between the LED and the access window. The camera (pco.1600 with Micro-NIKKOR 105 mm *f*/2.8 lens) is mounted on a horizontal slide, within an endoscopic access pipe. The camera's field of view is redirected vertically upwards with an optical mirror through a glass-covered recess in the intermediate floor. With this setup, the velocities inside the vortex core region can be measured at a height of h = 1.10 m above the pump intake, equaling a distance of Δh = 0.4 m from the water surface. A sketch of the setup can be seen in Fig. 4.

Since the LED beam fans out over the distance, the camera lens is set to a minimal focus depth by setting the aperture to *f*/2.8 in an attempt to minimize the error caused by the depth of field. The resulting pictures have a depth of field of ca. 2 cm. Camera and LED are synchronized by a microprocessor and controlled via a laptop, running the

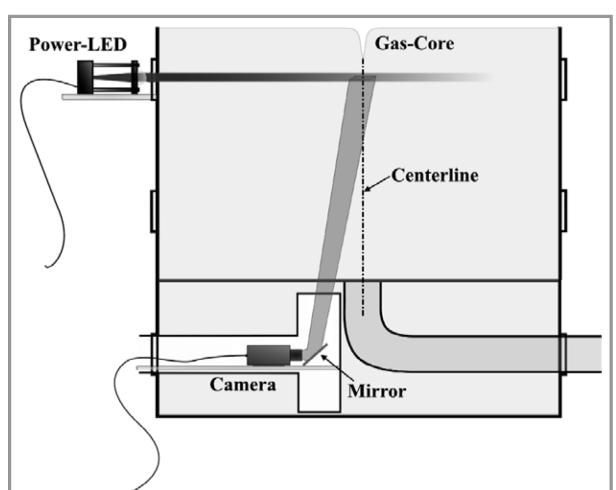

Figure 4. Setup for the particle image velocimetry measurements with high-power LED.

microprocessor and camera control software. Double-image recordings are done at a recording speed of 10 Hz, with a distance of Δt = 1 ms between the two images of a pair and an exposure time of t = 0.1 ms per picture. 600 double images are recorded, which equals a measurement time of 1 min. The recordings are evaluated with the PIVView software v3.6 from PIVTec, using a three-step multi-grid refining with a starting grid size of $128\times128\,\text{px}^2$, ending grid size of $64\times64\,\text{px}^2$ and 50 % overlap. Mean velocities are determined by combining the results of 20 double images. Since a mirror has to be used in the experiments to redirect the field of view, all images have to be deskewed in a preprocessing step, using the PIVMap 3 software from PIVTec.

4 Results and Discussion

4.1 Gas-Core Lengths

In Fig. 5, photographs of the different gas-core lengths are shown for measurements with the intermediate floor and a submergence depth of S = 1.5 m. The symmetric inflow conditions lead to a strong and stable vortex formation in all experiments. The resulting vortices can be seen as quasi-stationary with only minor fluctuations in the tip length of the forming gas cores. The maximum deviation from the mean gas-core length is 2.0 % for measurements with an open pump intake, while most experiments show fluctuations of below 1 %. The results for measurements without vortex suppressors are plotted in dimensionless form in Fig. 6 against the intake Froude number.

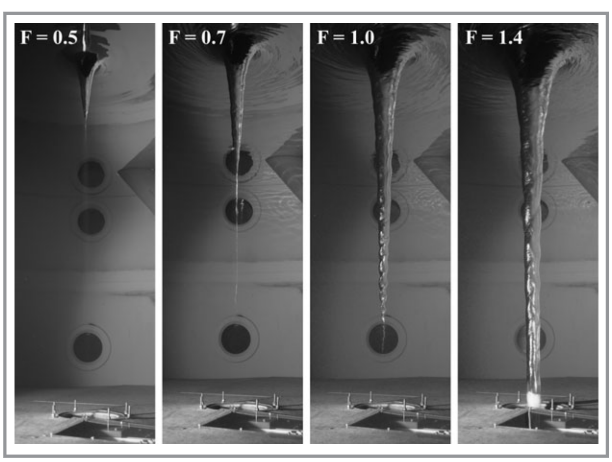

Figure 5. Photographs of the gas-core vortices for experiments with intermediate floor and S = 1.5 m.

The experiments conducted for the medium submergence depth of S = 1.5 m show that an intermediate floor has a negative, albeit minor influence on the gas-core lengths, reducing the critical Froude number from F = 1.5 to 1.4. This is most likely due to a higher symmetry as the pump intake pipe is below the floor and the overall smaller volume which has to be set in motion by the circulation.

Looking at the results for the open pump intakes, it is visible that for all investigated submergence depths, the development of the dimensionless gas-core lengths along the Froude number is sigmoid (S-shaped). Assuming that the difference in the circulation between the experiments is small and depending on the Froude number, the only difference in the experiments is the submergence depth S. Therefore, the development of the gas-core length can be described by a sigmoid equation of the form

$$L^* = \tanh \frac{CF^\alpha}{S} \tag{8}$$

The constant C and the exponent α are used to express the influence of the circulation on the vortex development. For all experiments with an open, unobstructed pump intake, the fitting constant C is 1 and the exponent α has a constant value of 2.8, showing the neglectable differences in the circulations between the varying submergence depths. The curves of the sigmoid functions are also plotted in Fig. 6 for the open pump intakes to show the good agreement with the experimental data.

Rearranging Eq. (8) makes it possible to calculate the Froude number for each submergence depth and gas-core length

$$F = \left(\frac{S}{C}\tanh^{-1}(L^*)\right)^{\frac{1}{\alpha}} \tag{9}$$

This further enables the possibility to calculate the critical Froude number by setting the gas-core length L^* to 1. Though it is better to use a defined cutoff value of 0.9 for L^*, as 1 is the upper asymptotic border for the sigmoid function and the deviation between the function and the experimental values increases for $L^* \rightarrow 1$. This also imposes an additional safety margin for the reliable operation of the pump system. With a constant value of L^* = 0.9, Eq. (9) can be simplified to

$$F_{90\%} = \left(\frac{1.472S}{C}\right)^{\frac{1}{\alpha}} \tag{10}$$

or in case for the experiments conducted with an open pump intake

$$F_{90\%} = (1.472S)^{0.357} \tag{11}$$

The resulting theoretical Froude numbers are $F_{90\%}$ (S = 1.1 m) = 1.2, $F_{90\%}$ (S = 1.5 m) = 1.3, and $F_{90\%}$ (S = 2.1 m) = 1.5 are in good agreement when compared to the measured Froude numbers $F_{90\%}^{\text{exp}}$ (S = 1.5 m) = 1.4 and $F_{90\%}^{\text{exp}}$ (S = 2.1 m) = 1.5. Note: The largest dimensionless gas-core length for S = 1.1 m is L^* = 0.84 at F = 1.10, which is less than the required 90 %. Therefore, the results for this submergence depth are excluded from comparison.

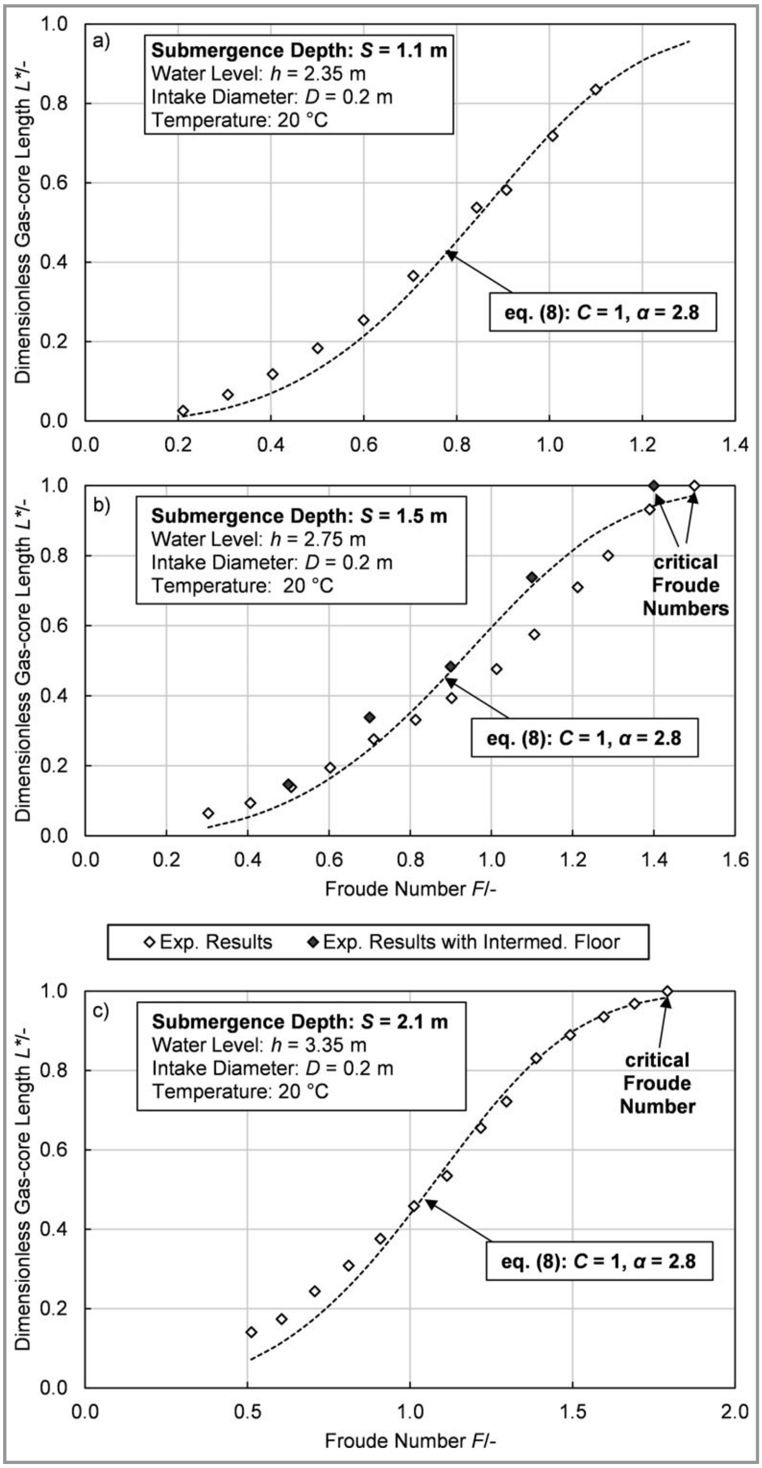

Figure 6. Dimensionless gas-core lengths for open tube pump intakes at a) S = 1.1 m, b) S = 1.5 m, and c) S = 2.1 m.

4.2 Vortex Suppressors

The experiments conducted with vortex suppressors show that the use of a funnel or 45° bend inlet have no significant impact on the gas-core length, as is evidently shown in Fig. 7a. The implemented sieve even has a negative impact on the inflow conditions, leading to a lower critical Froude number. This is most likely caused due to its shape, which reduces the intake area and, therefore, results in a higher intake velocity compared to the open pump intake at the same Froude number. The cross and cross-baffle devices on the other hand are found to be very efficient vortex suppressors, preventing gas entrainment even for large Froude numbers. The gas-core lengths of the experiments conducted with cross and cross-baffle vortex suppressors are plotted in Fig. 7 against the Froude numbers for submergence depths of S = 1.1 and 1.5 m.

By design, a volume flow rate of $Q = 755\,m^3h^{-1}$, resulting in a Froude number of F = 4.8, is the highest volume flow rate at which the plant can be safely operated. Therefore, no critical submergence is measureable for the cross and cross-baffle-shaped vortex suppressors, as the critical Froude number for them is considerably higher than 4.8. Nonetheless, sigmoid curves according to Eq. (8) can be fitted to each vortex suppressor and submergence depth. Unlike for the open pump intake, the values for C and α do not stay constant but change for each suppressor and also for each submergence depth. The exact values are listed in Tab. 2.

For the cross baffle with a diameter of 4D, no fitting is made, as too few gas-core lengths can be recorded for a meaningful fit before the maximum volume flow rate is reached. For the cross and cross-baffle vortex suppressors, no gas entrainment is observed during all experiments, while experiments without vortex suppression are limited to volume flow rates of $Q < 160\,m^3h^{-1}$ to avoid gas entrainment. As a result, the use of vortex suppressors with cross or even better cross-baffle shape enable a more than 3.5 times higher volume flow rate compared to an open tube pump intake. The efficiency increase is actually higher but cannot be exactly determined due to the limitations of the experimental setup. The maximum measurement uncertainty for the measurements with vortex suppressors caused by fluctuations of the gas-core length is 3.9 %, while again most experiments have deviations from the mean, which are below 1 %. Additionally, it is observed in measurements with cross-shaped suppressors, that the gas-core tip is lacerated at higher Froude numbers, which complicates the determination of the tip end slightly.

The reason behind the vortex suppressors' efficiency is made evidently when coloring the vortex core region with

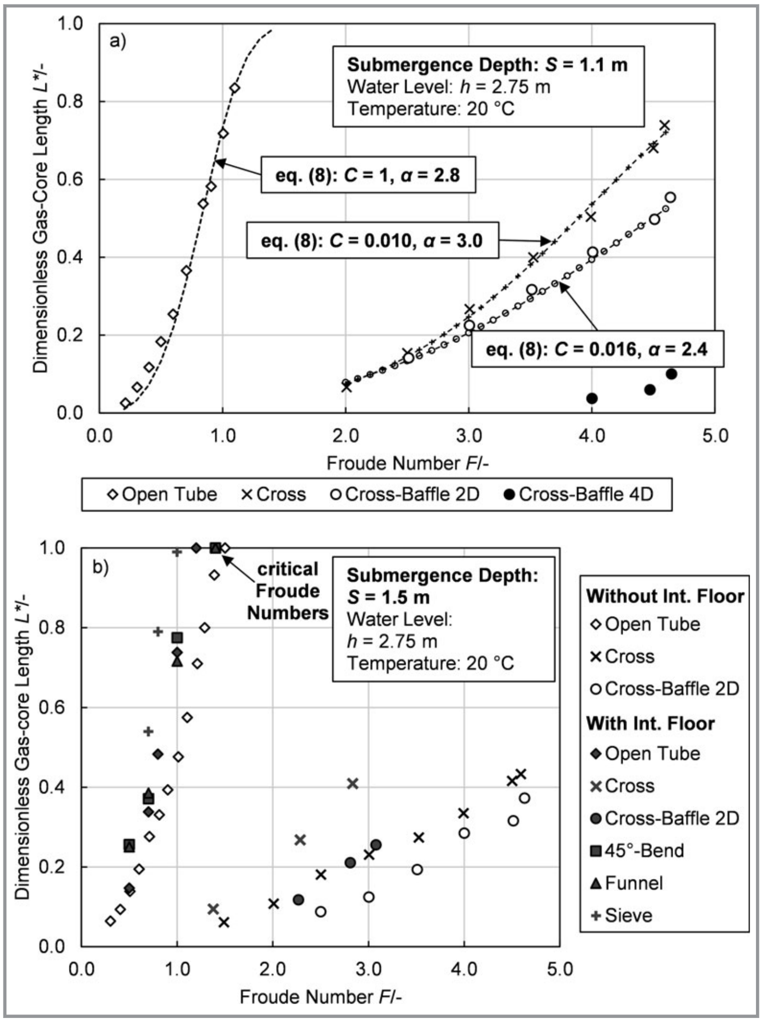

Figure 7. Dimensionless gas-core lengths for different vortex suppressors and open tube at a) S = 1.1 m and b) S = 1.5 m.

Table 2. Fitting parameters for vortex suppressors with a diameter of 2*D*.

Vortex Suppressor	S [m]	C [m]	α [–]
Cross 2*D*	1.5	0.032	2.00
	1.1	0.010	3.00
Cross Baffle 2*D*	2.1	0.016	1.95
	1.5	0.016	2.30
	1.1	0.016	2.40

dye, as can be seen in Fig. 8 for the open pump intake and the cross-baffle 2*D* vortex suppressor. While the vortex core region for the open pump intake is roughly 1/5 of the diameter of the pump intake wide, the vortex core diameter increases to the diameter of the baffle when using a cross-baffle-shaped vortex suppressor. As a result, the pressure drop causing the gas core to form is distributed over an area which is 100 times larger, leading to a wider but much shorter gas core. At the same time, the baffle is obstructing the straight line from the surface to the intake, resulting in a more radial intake of water instead of vertical, further reducing the vortex strength.

4.3 Azimuthal Velocity Profiles

From the PIV results of the measurements, a mean azimuthal velocity profile is derived and compared to numerical simulations. The simulations are conducted by the TÜV NORD EnSys GmbH & Co. KG using Ansys CFX [20]. Both experimental and numerical results can be seen in Fig. 9a plotted along the radius. Comparing the plots shows that the experimentally and numerically derived azimuthal velocities are in good agreement. Although the mean azimuthal velocities of the experiments are in general a bit lower than the numerical ones, they are almost all within close proximity. For most measurement points, the numerical results of the nearest height are within the standard deviation of the experimental results. Using Eqs. (2) and (3) for the calculation of the bulk circulation and the downward acceleration results in $\Gamma_\infty^{\text{exp}} = 0.3\,\text{m}^2\text{s}^{-1}$ and $a^{\text{exp}} = 2.7 \cdot 10^{-3}\,\text{s}^{-1}$ for the experiments and $\Gamma_\infty^{\text{CFD}} = 0.4\,\text{m}^2\text{s}^{-1}$ and $a^{\text{CFD}} = 2.8 \cdot 10^{-3}\text{s}^{-1}$ for the numerical simulation. From bulk circulation and axial acceleration, the theoretical gas-core length can be calculated for the experimental and numerical data using Eq. (4). Due to the difference in the values of the bulk circulation between experiments and simulations, the

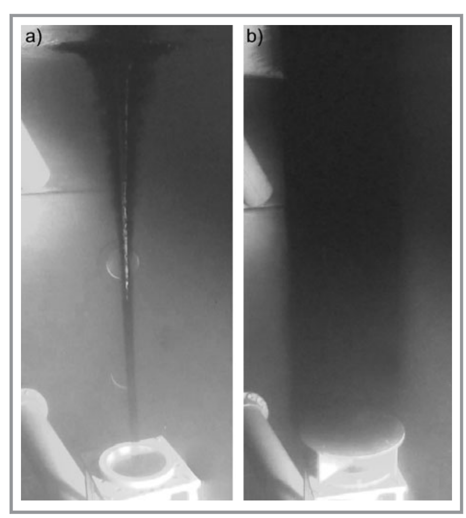

Figure 8. Visualization of the vortex-core region with blue ink: a) open pump intake and b) 2*D* cross-baffle vortex suppressor.

resulting theoretical gas-core lengths are $L^{\mathrm{BR,exp}} = 0.11\,\mathrm{m}$ and $L^{\mathrm{BR,CFD}} = 0.20\,\mathrm{m}$. The difference in the circulation values is caused by the limited field of view in the PIV measurements, as the circulation within the observable area has not yet reached the value of the bulk circulation (Fig. 9b). Nonetheless, the results of the numerical circulation are in very good agreement with the average measured gas-core length of $\bar{L}^{\mathrm{exp}} = 0.19\,\mathrm{m}$ or $\bar{L}^{*,\mathrm{exp}} = 0.13$, proving that the Burgers-Rott model is applicable for this setup and can be used to predict the occurring gas-core lengths. Further prove is provided by numerical simulations, conducted by the TÜV NORD EnSys GmbH & Co. KG for $F = 1.0$ and $S = 1.5\,\mathrm{m}$ [20], by comparing the calculated surface curvature with the experimentally measured gas-core lengths (Fig. 10).

Overall, the experiments prove to be challenging due to the large-scale measurement setup. The largest issue is the loss of light, stemming from the long distances between the light source, measurement area, and camera. Furthermore, the seeding particles are accumulating in the center of the vortex core, which leads to uneven particle distributions and an unresolvable vortex center. Ultimately, experiments could only be conducted successfully for $F = 0.5$, since the forming gas core is superseding the vortex core for larger Froude numbers. Due to reflections at the forming gas core, PIV measurements in the vicinity of the vortex core are rendered impossible.

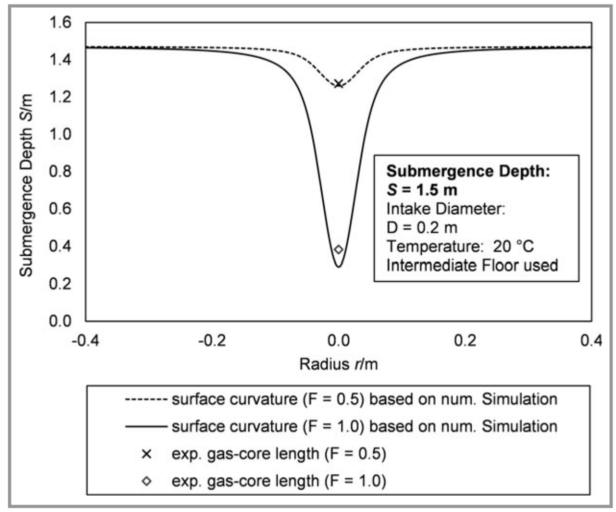

Figure 10. Comparison of numerically determined surface curvature with measured gas-core lengths.

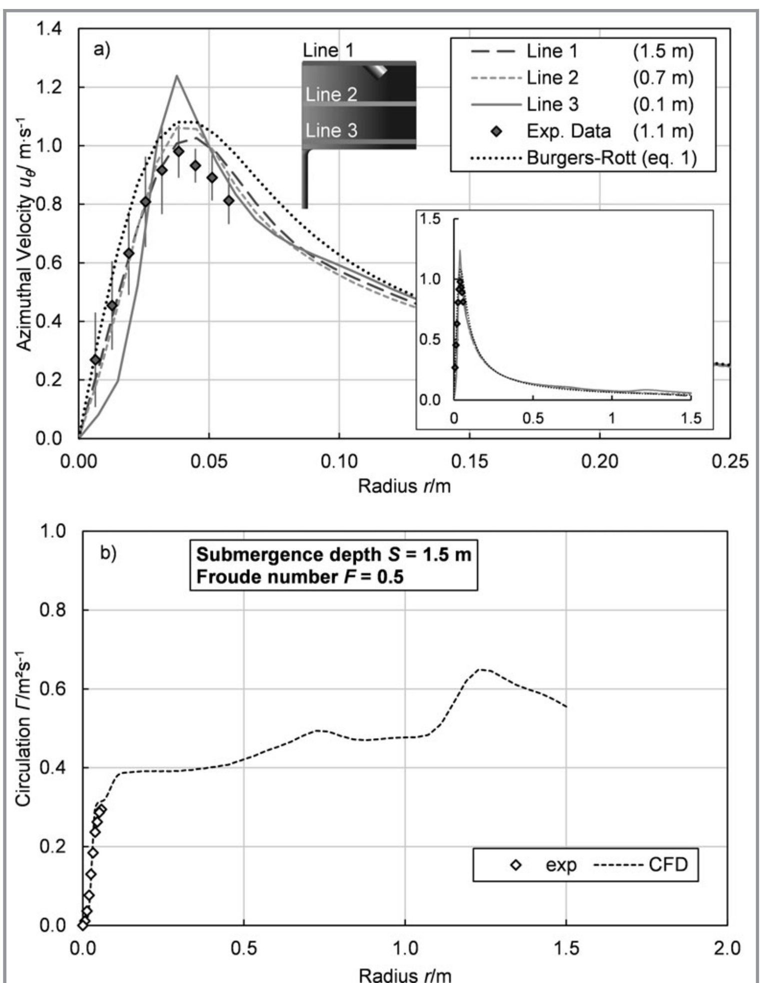

Figure 9. Experimental and numerical results for a) the radial profile of the azimuthal velocity and b) the circulation at $F = 0.5$.

5 Conclusions

To analyze the development and prevention of surface vortices in presence of strong circulations, experiments are carried out in a large-scale, cylindrical vessel at the Hamburg University of Technology. The measurement results show a sigmoid dependency of the gas-core length on the Froude number. For this dependency, an equation for the gas-core length is derived, consisting of the Froude number, the submergence depth, and two fitting parameters, representing the influence of the circulation. The equation is then used to derive a correlation for the critical Froude number, depending on the submergence depth and the two fitting parameters. For the open tube pump intake, only the submergence depth S is needed to calculate the critical Froude number. The experiments conducted with different vortex suppressors show that cross- and cross-baffle-shaped vortex suppressors are very effective in preventing gas entrainment into the pump system. Thereby, they drastically hinder the gas-core formation to the point that no critical Froude number can be reached within the observable measurement range. Additionally, the vortex suppressors are simple constructions, which can be easily implemented onto (existing) pump intakes.

In a second set of experiments, particle image velocimetry measurements to determine the velocity field inside the vortex core region are successfully conducted. For the measurements, a novel high-power LED system is implemented, improving the safety of the conducted experiments. The PIV results are used to validate numerical simulations and the theoretical vortex model of Burgers-Rott. Both the experimental and the numerical results show good agreement with the improvement of the Burgers-Rott vortex model made by Ito et al.

The project upon which this publication is based was funded by the German Federal Ministry of Education and Research under Project Number 02NUK023A. All experimental data used during the study are available from the corresponding author by request.

Symbols used

a	[s^{-1}]	downward acceleration
C	[m]	fitting constant, Eq. (8)
D	[m]	pump intake diameter
D_P	[µm]	seeding-particle diameter
F	[–]	Froude number
$F_{90\%}$	[–]	Froude number at $L^* = 0.9$
g	[m s^{-2}]	gravitational acceleration
h	[m]	height
L	[m]	gas-core length
L^*	[–]	dimensionless gas-core length
Q	[m^3h^{-1}]	volume flow rate
r	[m]	radius
r_0	[m]	vortex-core radius
S	[m]	submergence depth of pump intake
S_{crit}	[m]	critical submergence depth at $L^* = 1$
t	[ms]	time
u	[m s^{-1}]	pump intake velocity
u_θ	[m s^{-1}]	azimuthal velocity

Greek letters

α	[–]	fitting exponent, Eq. (8)
β	[°]	vertical inflow angle
Γ	[m^2s^{-1}]	circulation
Γ_∞	[m^2s^{-1}]	bulk circulation
λ	[nm]	wave length
ν	[m^2s^{-1}]	kinematic viscosity
ρ	[kg m^{-3}]	density

Sub- and superscripts

BR	superscript used to denote values calculated with Burgers-Rott model (Eq. (4))
CFD	superscript used to denote numerical data
exp	superscript used to denote experimental data

Abbreviation

PIV	particle image velocimetry

References

[1] J. Knauss, *Wirbelbildung an Einlaufbauwerken – Luft- und Dralleintrag*, Schriftenreihe des Deutschen Verbandes für Wasserwirtschaft und Kulturbau e.V., Vol. 63, Paul Parey Publishing, Berlin **1983**.

[2] G. E. Hecker, W. W. Durgin, The Modelling of Vortices at intake Structures, *IAHR-ASME-ASCE Joint Symposium on Design and Operation of Fluid Machinery*, Fort Collins, CO, June **1978**.

[3] H. O. Anwar, Flow in a Free Vortex, *Water Power* **1965**, *4*, 153–161.

[4] H. O. Anwar, Prevention of Vortices at Intakes, *Water Power* **1968**, *10*, 393–401.

[5] L. L. Daggett, G. H. Keulegan, Similitude Conditions in Free-Surface Vortex Formations, *J. Hydraul. Div., Am. Soc. Civ. Eng.* **1974**, *100*, 1565–1581.

[6] A. K. Jain, K. G. Ranga Raju, R. J. Garde, Vortex Formation at Vertical Pipe Intakes, *J. Hydraul. Div., Am. Soc. Civ. Eng.* **1978**, *104*, 1429–1445.

[7] A. J. Rindels, J. S. Gulliver, *An Experimental Study of Critical Submergence to Avoid Free-surface Vortices at Vertical Intakes*, Project Report No. 224, University of Minnesota, Minneapolis, MN **1983**.

[8] J. Keller, G. Möller, R. M. Boes, PIV Measurements of Air-Core Intake Vortices, *Flow Meas. Instrum.* **2014**, *40*, 74–81.

[9] W. J. M. Rankine, *A Manual of Applied Mechanics*, Richard Griffin and Company, London, **1858**.

[10] J. Burgers, A Mathematical Model Illustrating the Theory of Turbulence, *Adv. Appl. Mech.* **1948**, *1*, 171–199.

[11] N. Rott, On the Viscous Core of a Line Vortex, *Z. Angew. Math. Phys.* **1958**, *9*, 543–553.

[12] K. Ito, T. Sakai, Y. Eguchi, H. Monji, H. Ohshima, A. Uchibori, Y.Xu, Improvement of Gas Entrainment Prediction Method, Introduction of Surface Tension Effect, *J. Nucl. Sci. Technol.* **2010**, *47*, 771–778.

[13] A. J. Odgaard, Free-Surface Air Core Vortex, *J. Hydraul. Eng.* **1986**, *112*, 610–620.

[14] *American National Standard for Rotodynamic Pumps for Pump Intake Design*, Hydraulic Institute, Parsippany, NJ **2012**.

[15] A. Auckland, I. Nistor, R. Townsend, Intake Shape and Boundary-Related Considerations in the Operation and Design of Storm-Sewer Drop Structures, *Can. J. Civ. Eng.* **2009**, *36*, 1825–1834.

[16] T. Trivellato, Anti-vortex Devices: Laser Measurements of the Flow and Functioning, *Opt. Lasers Eng.* **2010**, *48*, 589–599.

[17] S. M. Borgei, A. R. Kabiri-Samani, Effect of Anti-vortex Plates on Critical Submergence at a Vertical Intake, *Sci. Iran., Trans. A* **2010**, *17*, 89–95.

[18] M. Padamanabhan, *Evaluation of Vortex Suppressors, Hydraulic Performance of Single Outlet Sumps, and Sensitivity of Miscellaneous Sump Parameters*, Report No. 49A-82/M398F, Alden Research Laboratory, Inc., Holden, MA **1982**.

[19] N. Szeliga, D. Bezecny, S. Richter, M. Schlüter, *Schlussbericht Verbundprojekt SAVE: Sicherheitsrelevante Analyse des Verhaltens von Armaturen, Kreiselpumpen und Einlaufgeometrien unter Berücksichtigung störfallbedingter Belastungen – Teilprojekt A*, Technische Universität Hamburg-Harburg, Hamburg **2017**.

[20] F. Blömeling, R. Lawall, *Schlussbericht Verbundprojekt SAVE: Sicherheitsrelevante Analyse des Verhaltens von Armaturen, Kreiselpumpen und Einlaufgeometrien unter Berücksichtigung störfallbedingter Belastungen – Teilprojekt C: Analytische Untersuchungen der Wirbelbildung in Pumpeneinläufen*, TÜV NORD EnSys GmbH & Co. KG, Hamburg **2017**.

